Durable low ice adhesion foams modulated by submicron pores

Journal:	*Industrial & Engineering Chemistry Research*
Manuscript ID	ie-2019-02939x.R2
Manuscript Type:	Article
Date Submitted by the Author:	31-Aug-2019
Complete List of Authors:	Li, Tong; Norwegian University of Science and Technology, Department of Structural Engineering Zhuo, Yizhi; Norwegian University of Science and Technology, Department of Structural Engineering Håkonsen , Verner; Norwegian University of Science and Technology, Department of Structural Engineering He, Jianying; Norges teknisk-naturvitenskapelige universitet, Zhang, Zhiliang; Norges teknisk-naturvitenskapelige universitet,

Durable low ice adhesion foams modulated by submicron pores

Tong Li, Yizhi Zhuo, Verner Håkonsen, Jianying He and Zhiliang Zhang**

NTNU Nanomechanical Lab, Department of Structural Engineering, Norwegian University of Science and Technology (NTNU), 7491, Trondheim Norway.

E-mail: jianying.he@ntnu.no and zhiliang.zhang@ntnu.no

Keywords: elastomeric foam, icephobicity, porous PDMS, submicron porous elastomer, mechanical robustness, chemical stability

Graphical abstract

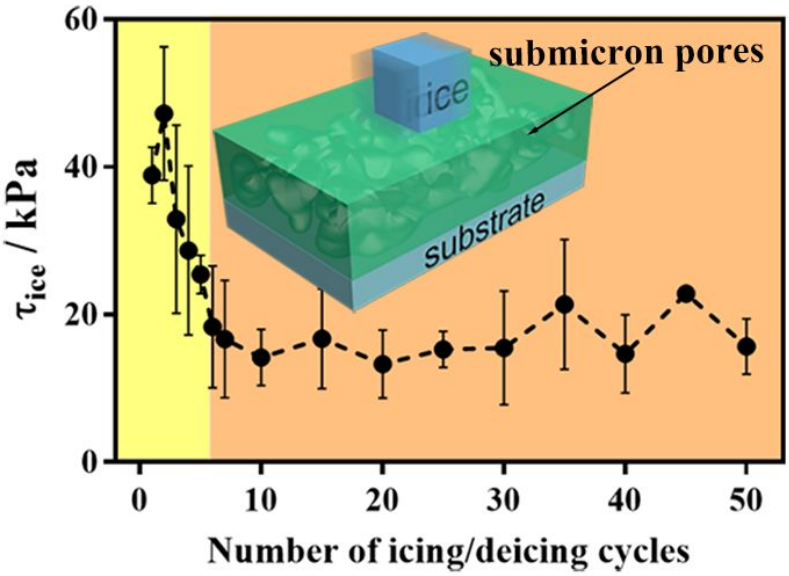

Abstract

Ice accretion is a severe challenge for both production and livelihood in cold regions. Previously reported high-performance icephobic surfaces by infusing lubricants are either temporarily icephobic, chemically unstable or mechanically weak. Herein, we report the design and fabrication of submicron porous polydimethylsiloxane (PDMS, Sylgard 184 with weight ratio 10:1) foams based chemically stable and mechanically robust icephobic materials. The relationship between the ice adhesion strength and porosity is revealed. Without any surface additives and lubricants as well as sacrificing the crosslinking density of elastomeric foam, the stable ice adhesion strength of the submicron porous foam reaches 16.8 ± 5.8 kPa after 50 icing/deicing cycles. In addition, the icephobic foams show excellent chemical stability and mechanical robustness, and the ice adhesion strengths are all less than 30.0 kPa after acid/base/salt/organic solvent corrosion and 1000 abrasion cycles. The submicron porous elastomeric strategy opens up a new avenue for high-performance durable icephobic materials with excellent stability and robustness.

1 Introduction

Ice accretion can cause severe problems for infrastructures and transportations, such as collapse of grid infrastructures, failure of turbine blades and traffic accidents as well as malfunctioning in solar cells.[1-5] Conventionally, thermal, mechanical and chemical approaches are adopted to tackle these challenges, including heating iced surfaces, salting on roads and directly removing ice by force.[6-8] These active methods, however, result in either excess energy consumption or environmental pollution.[9] Hence, there remains a strong need to develop passive methods for effective deicing.

According to the interfacial adhesion mechanics, the average shear stress required to separate the rigid object (*e.g.* ice) from a soft homogeneous coating is given as[6, 10, 11]

$$\tau \propto \sqrt{\frac{W \times G}{t}}$$

where τ is the shear strength, W is the work of adhesion, t is the thickness of the coating, and G is shear modulus. Apparently, if the values of W and G decrease, and t increases, the corresponding τ reduces.

Icephobicity can be defined by the ice adhesion strength of the surfaces. If the ice adhesion strength is below the threshold of 100 or 10 kPa, the surfaces can be referred as an icephobic or super-low ice adhesion surface, respectively.[11, 12] In the past years, several approaches, including decreasing water crystallization temperature,[13, 14] delaying freezing time,[15-20] and lowering ice adhesion strength of surfaces,[2, 6, 11, 12, 21, 22] have been adopted to create passive icephobic surfaces. In particular, superhydrophobic surfaces have been extensively investigated aiming to prevent super-cooled water from freezing on surfaces, but the mechanical properties and/or interlocking effect of these textured surfaces are still the challenges for icephobicity, restricting their application perspective.[23-25] Recently, lubricants-

infused surfaces were developed, including the slippery[26-31] and slippage-induced[1, 11] surfaces, to achieve low ice adhesion strength so that the accumulated ice can be easily removed by self-gravity of ice or winds. Since there exists a layer of lubricant on the slippery surface, the accumulated ice does not contact with the solid surface directly. Consequently, the ice adhesion strengths of the slippery surfaces are significantly reduced because of the intrinsic low shear modulus of lubricants.[13, 28, 29] However, the sacrificial nature of lubricants results in poor durability of the icephobicity. Furthermore, icephobic surfaces with infusing miscible lubricants by slippage mechanism are developed to tackle the poor durability of the slippery icephobic surfaces.[1, 11] Low shear modulus surfaces with durable and high icephobicity were obtained by tailoring the crosslinking density of different polymeric coatings with miscible oils and enabling interfacial slippage.[1, 6, 11] However, if the crosslinking density is sacrificed greatly, the polymers are not easy to form a solid state.[6] Their mechanical properties and physical/chemical properties become new issues. For example, the low crosslinking polymers could be more viscous and easier to degrade than the high-crosslinking polymers;[32, 33] and sacrificing crosslinking density of the coatings resulted in obvious thickness loss when testing the anti-abrasive property.[11] In addition, the lubricant could be depleted if the surfaces contact the outer chemicals (e.g. organic solvent) for the lubricant-infused surfaces. In our previous work, Sylgard 184 sponge with sub-millimeter scale pores and extra curing agent (more than the weight ratio of 9.1%) was developed. It showed stable ice adhesion about 1 kPa even after 25 icing-deicing cycles.[12, 34] The super-low ice adhesion strength is attributed to the coupling effect of increase in total crack length, decrease in elastic modulus, reduction in surface energy and enabled slippery effect.[11, 12, 34] So far, the effect of the solo pore for lowering the ice adhesion strength have not been investigated.

To overcome the intrinsic limitations of the previous strategies (Figure 1a-d), and inspired by the effective medium theory,[35] here we present the submicron porous elastomeric strategy for

durable icephobicity (Figure 1e). The apparent shear modulus of the porous elastomeric foam is between the shear modulus of the air and the solid elastomer, which is governed by the intrinsic properties of the matrix materials and the porosity. In general, the apparent shear modulus decreases with the increase of the porosity.[36] On the other hand, according to the adhesion failure theory,[6, 12, 37] the decrease of shear modulus of foam increases the mismatch with ice and reduces its ice adhesion strength. Without any surface additives and lubricants as well as sacrificing the crosslinking density of elastomer, the stable ice adhesion strength of the obtained submicron porous foam reaches ca. 16.8 ± 5.8 kPa after 50 icing/deicing cycles, demonstrating durable icephobicity. Moreover, the ice adhesion strengths of the submicron porous foams are below 30.0 kPa after acid/base/salt/organic solvent corrosion and 1000 abrasion cycles, showing excellent chemical stability and mechanical robustness. In addition, we demonstrate that the submicron porous elastomeric foams have low apparent elastic modulus with normal crosslinking density (Sylgard 184 with weight ratio 10 : 1). The lubricant-free submicron porous elastomeric foams provide a facile and novel strategy to enable high-performance durable icephobicity with mechanical robustness and chemical stability.

2 Results and discussion

2.1 The submicron porous elastomeric foams

Figure 1e shows the fabrication route of the submicron porous foams. The hybrid surfactant (Span 80 and Tween 80) as the porogen is dispersed in the Sylgard 184 component with a weight ratio of 10 : 1, forming an emulsion system. The obtained fluid is then coated on the substrates. After storing the precursors on substrates at 65 ^{o}C for 4 h, all of them become solid state completely. Then in the removing porogen process, the hybrid solvent (ethanol/water) is selected to remove the porogen (hybrid surfactant), as ethanol/water mixture can dissolve the hybrid surfactant and PDMS can slightly swell in ethanol.[38] Finally, the submicron porous

foams are formed when the solvent is removed by a heating process (the areas of the foams change negligibly before and after removing the porogen). The obtained foams are marked as 0 - 50% corresponding to the weight ratio of porogen to the total precursors. Notably, when the porogen is introduced into the Sylgard 184, the fluidity of the hybrid precursors decreases in the porogen weight ratio range of 0 - 50%, increasing the difficulty in forming the foams. In particular, the 30% sample is a compromise between the porosity and the ability to form submicron porous foams. The porosity of the samples is estimated based on the equation P (porosity) = $1 - V_{framework} / V$, where $V_{framework}$ is the volume of PDMS and can be calculated by weight of samples diving density of pristine PDMS, and V is the volume of samples.[39] The obtained porosity of the samples varies from 0 – 48.4% (Table 1). The structures of pristine Sylgard 184 PDMS, 10, 20, 30, 40 and 50% samples are further revealed by their SEM images (Figure 2). In contrast to the pristine Sylgard 184 samples, the 10 - 50% samples exhibit isolated or continuous submicron porous structures. The average pore sizes of 10 - 50% samples are ca. 489.6 ± 134.3, 482.6 ± 144.5, 483.9 ± 154.6, 470.7 ± 134.6 and 609.9 ± 96.6 nm, respectively (Figure S1), and the shapes of pores vary from isolated to continuous porous structures. The large value of the errors of the pore size is attributed that not all the pores were cut through the center of pores. It should be noted that the pore size of 50% sample is defined as the distance between the ridges. In addition, in contrast to the optical images of pristine PDMS (Figure S2a), the optical microscopy images (Figure S2b-d) of these 10 – 50% samples also indicate the pores are formed. Moreover, as shown in Figure S3, the surfaces of 0 - 40% samples are flat without pores, revealing the pores of these samples are packed in the inner space of the foams. The pores of 50% sample appear at the surface of the foam, due to a large amount of porogen used.

The surface morphology and structure of the 30% sample are further investigated and analyzed as a typical sample in detail. The top-view SEM image (Figure 3a) shows that the foam is smooth with shallow dents uniformly distributed on the surface, where the average

diameter of these dents is estimated to be 610 nm. The AFM images further demonstrate the smooth top surface has an RMS roughness of 28 nm from an area of 10 μm × 10 μm. The depth of the dents is estimated as *ca.* 28 nm by the AFM images (a height profile is shown in Figure S4 as an example), indicating the dents are quite shallow and the surface is rather flat. Although the RMS roughness of 30% sample is higher than the pristine Sylgard 184 surface (Figure S5, RMS roughness of 2.4 nm, 10 μm × 10 μm), it is much lower than many porous surfaces (*e.g.* Figure S6, porous surfaces can result in interlocking effect for ice in harsh humidity).[8, 24, 27] Moreover, the cross-sectional SEM image (Figure 3b) and optical microscopy image (Figure 3e) show that the pores are packed inside the foam. The pore size is roughly estimated to be *ca.* 450.2 ± 135.5 nm based on the SEM image (Figure 3b). Hence, the foam has a relatively smooth surface with pores inside the structure. The images of the submicron porous foams with a thickness of 50 μm and 1 mm further demonstrate that the surface morphology of submicron porous foam is homogeneous (Figure 3f and g). Unlike icephobic Sylgard 184 sponge in which the thickness is larger than sub-millimeter (corresponding to the pore size in sponge),[34, 40] the thickness of the submicron porous foams can be regulated from micrometer-scale to millimeter-scale. In addition, the wettability of the 30% sample is revealed in contrast to pristine PDMS surface. As shown in Figure S7, the water contact angle of the 30% sample (114.7 °) is slightly higher than the pristine Sylgard 184 PDMS (111.4 °), which may due to the higher RMS roughness of 30% sample surface than the pristine Sylgard 184 surface.

2.2 Effect of weight ratio of porogen on apparent shear modulus and ice adhesion strength.

According to the adhesion failure theory, shear modulus is one of the significant factors related to ice adhesion strength. To reveal the relationship between ice adhesion strength and apparent shear modulus of submicron porous foams, different porosity of Sylgard 184 samples with the same thickness (*ca.* 50 μm) are prepared by regulating the weight ratio of porogen to Sylgard 184 component. Their mechanical properties are further investigated by the flat punch

nanoindentation tests. The obtained unloading stiffness and corresponding apparent shear modulus are shown in Figure 4b and Table 1 (The calculation processes for apparent shear modulus are shown in the supporting information). Comparing to the shear modulus of 0.80 MPa for pristine Sylgard 184 PDMS, the apparent shear modulus of the submicron porous foams dramatically decrease to a value smaller than 0.35 MPa. However, the shear modulus declines slowly with further increasing porosity. When the weight ratio of porogen to elastomer exceeds more than 60%, distinct phase separation occurs for the hybrid precursors, and no practical foams form (Figure S8).

The relationships between ice adhesion strength, porosity and apparent shear modulus are then revealed. Since there may exist severe interlocking effect for ice of 50% sample because of its surface pores (Figure S3f), the relationships are revealed based on the 0 - 40% samples. Notably, the value of ice adhesion strength reduces as the probe velocity decreases,[10] so the ice adhesion strengths of the samples need to be compared with the value of pristine Sylgard 184 sample at the same testing condition. As shown in Figure 4b, the ice adhesion strength decreases with the increase of the weight ratio of porogen. The relationship between apparent shear modulus and ice adhesion is further illustrated as $\tau_{ice} = \sigma\sqrt{G} + b$, where $\sigma = \sqrt{w/t} = 35$ $kPa^{0.5}$ and b = - 547.0 kPa, where σ and b are the slope and intercept of the fitted curve in Figure 4c. It should be noted that the mechanical performance of pristine Sylgard 184 sample is quite different from the porous foams, so it is used as a control sample while not included in the curve fitting in Figure 4c.

Furthermore, the relationship between ice adhesion strength and apparent shear modulus is revealed in Figure 4 c and d. In detail, the normalized ice adhesion strength and normalized shear modulus for pristine Sylgard 184 coating are all denoted as 1; and the normalized results for the 10 - 50% coatings are denoted as the ratio of ice adhesion strength/shear modulus of

samples to the value of pristine Sylgard 184 coating. From the fitted curves and equation (Figure 4c and d), it is clear that the ice adhesion strength decreases greatly with the introduction of pores. The intrinsic mechanism can be explained by the stiffness mismatch promoted interface failure between ice and elastic polymers, which is governed by the crack initiation and propagation during the deicing process [41-43].

2.3 Durability, stability and mechanical properties of submicron porous foams

To demonstrate the practical applications of the submicron porous icephobic material, its durability for icephobicity is tested by the cyclic icing/deicing tests. The 30% submicron porous sample with a thickness of 1 mm is used as the optimal sample for durability and stability investigation of the submicron porous foam. As shown in Figure 5a, the ice adhesion strength of submicron porous foam decreases from 39.1 kPa to 18.3 kPa during the initial 5 cycles, and then kept stable within 50 cyclic tests. The SEM image of the surface after 5 icing/deicing cyclic test is shown in Figure S10a, indicating the morphology changes after the icing/deicing cycles. Then, in the following icing/deicing cycle tests, the structure of the surface has been stable and less sensitive to the outer force, the ice adhesion strength keeps steady within 50 cyclic tests, showing remarkable mechanical durability of the icephobicity. The stable ice adhesion strength of the 30% submicron porous foams are obtained as 16.8 ± 5.8 kPa based on analyzing the ice adhesion strengths after the fifth cycle. To the best of our knowledge, such low ice adhesion strength is the lowest value for lubricant-free Sylgard 184 samples with a normal weight ratio of 10:1. It is predictable that submicron porous elastomers could reach even lower ice adhesion strength if suitable porosity and/or elastomers are selected. The icephobic materials should endure not only icing/deicing cycle tests but also the harsh environment in outdoor applications. Herein, acid (hydrochloric acid, 2 M), base (NaOH, 2 M), salt (NaCl, 2 M) aqueous solutions and an organic solvent (hexane) are used as corrosion mediums to evaluate the chemical stability of the icephobic submicron porous foams. The 30%

samples are soaked in corresponding solutions for 12 h, and then their wettability and ice adhesion strengths are tested. As shown in Figure 5b, compared to 114.7 º before soaking, the water contact angles of the 30% samples decrease to 114.5 º (acid), 110.4 º (base), 111.6 º (salt) and 114.1 º (hexane) after soaking, respectively. The insignificant decrease of the water contact angles demonstrates favorable stability of the surfaces. The ice adhesion strengths of these samples after the corresponding soaking are 21.0 kPa (acid), 16.0 kPa (base), 14.1 kPa (salt) and 12.3 kPa (hexane), respectively (Figure 5c). These four kinds of typical liquid hardly influence the high-performance icephobic properties of the submicron porous samples, demonstrating excellent chemical stability.

In addition to the durability and stability of icephobic materials, the remarkable anti-abrasive property is also crucial for their practical applications. The sandpaper abrasion test on the submicron porous foams is conducted at a pressure of 1.5 kPa for their mechanical properties. Although the surface of the foams is scuffed (Figure S10 b and c), the submicron porous surface still has low ice adhesion strength below 30 kPa even after 1000 abrasion cycles with the 400-grit sandpaper (Figure 5c). Such high-performance icephobicity after abrasion test is associated with low apparent shear modulus of the submicron porous foams. When the shear force is exerted on the sample, the pores result in the easy deformation of the surface, alleviating the sandpaper grind off the sample.

2.4 Comparison of Sylgard 184 PDMS foams with bulk PDMS.

The icephobic durability, chemical stability and mechanical properties of the foams are compared with the bulk PDMS (non-pores). In detail, the foam PDMS (30% sample) and bulk PDMS sample (supporting information) with the same modulus (ca. 299 kPa) are used for comparison. As shown in Figure 6a, the initial ice adhesion of the bulk PDMS (ca. 17.5 ± 4.8 kPa) is lower than that of the foam sample with initial ice adhesion (39.1 ±3.8 kPa, Figure 5a),

but close to the foam PDMS with stable ice adhesion (after several icing/deicing cycles, ca. 16.8 ±5.8 kPa). After 10 icing/deicing cycles, the foam and the bulk PDMS have similar ice adhesion, both of which show durable low ice adhesion. Furthermore, the chemical stability of the foam and the bulk PDMS are compared by soaking the sample into organic solvent for 12 h. The ice adhesion of the bulk PDMS after soaking increases from ca. 18.1 to 41.8 kPa, whereas the ice adhesion of the foam is below 20 kPa. The chemical stability of the foam for icephobicity is much better than the bulk sample. In addition, the normalized weight loss of the bulk and foam PDMS samples during the abrasion tests are shown in Figure 6b. The foam sample shows a lower weight loss ratio than the bulk PDMS, showing better anti-abrasion properties than the bulk PDMS.

2.5 Comparison of Sylgard 184 PDMS foams with sub-millimetric pores and submicron pores.

The reported sub-millimetric icephobic materials and our submicron porous foams are compared based on their chemical stability. The samples with pore sizes of *ca.* 270 μm and *ca.* 450.2 nm are soaked in ethanol for 12 h and then dry at 80 ^{o}C for 1h, respectively. Figure 7 shows the SEM images and corresponding schematics of the sub-millimetric porous icephobic foams (Figure 7a and c) and our submicron porous foams (Figure 7b and d), respectively. In contrast to the submicron porous foams with a relatively smooth surface after soaking, the surface with sub-millimetric pore collapses. It is predictable that the severe deformation of the surface will result in a higher ice adhesion strength.

3 Conclusion

Building on the principles of reducing apparent shear modulus, we report the design and fabrication of submicron porous elastomeric foams (Sylgard 184 with weight ratio 10:1) based chemically stable and mechanically robust icephobic materials. As the porosity increases, the

ice adhesion strengths of the foams decrease. Remarkably, without any surface additives and lubricants as well as sacrificing the crosslinking density of the foam, the stable ice adhesion strength of the optimal submicron porous foam reaches *ca.* 16.8 ± 5.8 kPa after 50 icing/deicing cycles assessment. In addition, the ice adhesion strengths of the optimized icephobic foams are all less than 30.0 kPa after acid/base/salt/organic solvent corrosion and 1000 abrasion cycles, demonstrating excellent chemical stability and mechanical robustness. The submicron porous elastomeric foam strategy sheds new light on high-performance durable icephobic materials with excellent chemical stability and mechanical robustness.

4 Experimental section

Materials and chemicals.

Sylgard 184 kits were obtained from Dow Corning. Span 80, Tween 80, hexane, ethanol and other solvents were purchased from Sigma-Aldrich. All chemicals were used as received without further purification. Ultrapure water with a resistivity higher than 15.0 MΩ cm was used in all experiments. Glass substrates were cut into 5 cm × 5 cm ×2 mm.

Preparation of hybrid precursors.

Firstly, a silicone base and a curing agent of Sylgard 184 silicone elastomer by the weight ratio of A : B = 10 : 1 were mixed and stirred vigorously for 10 min, which was marked as the Sylgard 184 component. Then liquid Span 80 and Tween 80 with a weight ratio of 3 : 1 - 4 : 1 were mixed by ultrasound for 5 min at room temperature, which was marked as the porogen. The Sylgard 184 component and the porogen with different weight ratios (10 : 0 - 5 :5) were mixed, stirred vigorously for 10 min, and degassed for 30 min to remove air bubbles. Finally, the hybrid precursors (water-in-oil emulsion) form.

Preparation of icephobic foams.

The submicron porous foams were prepared by the following procedures. The hybrid precursors were drip-coated or spin-coated (WS-400B-6NPP-LITE/AS, Laurell Technologies) on the glass substrates for 30 s with a speed of 500 - 1000 rpm and thereafter for 30 s with the speed of 500 - 3500 rpm. After the samples were soaked into the mixture of water and ethanol (the volume ratio 1 : 1) for 6 h at 65 ^{o}C for three times to remove the porogen. Finally, the porous foams were obtained after drying in an oven at 80 ^{o}C for 3 h to remove the solvent (no mass changes after further drying process). A control sample with porous surface was prepared from the sample procedures as the icephobic foam, in which Span 80 was used as the porogen. The bulk PDMS samples (ca. 1 mm thickness) with different modulus was also prepared by regulating the weight ratio of Sylgard 184.

Characterization.

Scanning electron microscopy (SEM) was carried out in the field emission scanning electron microscope (FEI SEM APREO). All samples were sputter-coated with a 10 nm platinum/palladium layer. The surface morphology and roughness of the samples were recorded by Atomic Force Microscopy (AFM, Veeco Metrology) using PeakForce Quantitative NanoMechanics mode. Quasi-static nanoindentation tests were conducted in a TriboIndenter® 950 (Hysitron, Inc.) by using a cylindrical diamond flat punch with 53.70 ± 0.06 μm in diameter. The samples were loaded to the maximum load (P_{max}) in 5 s and then held in the P_{max} for 10 s, followed by unloading in 5 s. The P_{max} for each sample was 100 μN. Thicknesses of the samples were measured by an absolute digimatic indicator (Mitutoyo, ID-C112GB). The porosity of the samples was obtained based on the volume ratio of the framework to the total volume of the samples. The prepared pristine Sylgard 184 and 10 - 50% samples were cut into the cylindrical structures by a cylinder mold for measuring the height and the area of cylindrical base. The volume of the samples was calculated from the area multiplied by the height. Ice adhesion strength was measured by a universal mechanical tester

(Instron Model 5944) equipped with a home-made cooling system and chamber, as described in previous reports.[2] The corresponding schematic is shown in Figure S11. A polypropylene tube with 1 mm thick wall and 15.3 mm inner diameter was placed onto the samples acting as an ice mold, and then 5 mL deionized water (20 ^{o}C) was syringed into the tube. The sample was transferred into a freezer at -18 °C for more than 3 hours to ensure complete freezing. Before test, the samples with ice tube were placed into the cooling chamber and stabilized at -18 °C for 5 min. During the ice adhesion tests, a force probe with 5 mm diameter propelled the tube-encased ice columns under a velocity of 0.01 mm s^{-1}, with the probe aligned close to the tested sample surface (less than 2 mm) to minimize the torque on the ice cylinder. The loading curves were recorded, and the peak value of the shear force was divided by contact area to obtain the ice adhesion strength. In each icing/deicing cycle, 5 mL distilled water was added to the attached polypropylene on the sample surface and then kept at -18 °C for at least 3 hours horizontally to ensure icing, and then the sample was quickly transferred to the cooling chamber to test the ice adhesion strength, which was designated as one cycle. After the ice adhesion test, the same procedure was applied for the next cycle and the water with tube was always placed to the same position on the sample surface. The total icing/deicing tests were carried out for 50 cycles. The chemical stability tests were performed by soaking the samples into hydrochloric acid (2 M), NaOH (2 M), NaCl (2 M) aqueous solutions and hexane for 12 h. After soaking, the samples were rinsed by deionized water and dried for water contact angle (WCA) measurements and ice adhesion tests, respectively. In detail, the samples soaked in hydrochloric acid, NaOH and NaCl aqueous solution were blow-dried by nitrogen for ca. 3 min; the sample soaked in hexane was dried by evacuation for 1 h. Then the WCA values were measured on a Drop Shape Analyzer - DSA 100 at ambient temperature. For the ice adhesion test after soaking, the samples were rinsed and dried at 60 ^{o}C to remove the solvent on the surface and inside. The abrasion tests were performed at about 30 cycles min^{-1} with the 400-

grit sandpaper based on the previous method.[6] In detail, the cylindrical load was covered with sandpaper on its round bottom, and the pressure is calculated as 1.5 kPa. Then the load with sandpaper side was placed face down on the samples and moved horizontally on surfaces of the samples for 5 cm, in which one moving across the sample was recorded as one abrasion cycle. The root-mean-squared roughness of the 30% sample before and after 50 icing/deicing cycles were measured by a profilometer (Dektak 150) from a horizontal distance of 2 mm.

Supporting Information

The Supporting Information is available on the website.

Apparent shear modulus of the coatings, mechanical properties of the bulk PDMS and the smooth and porous surfaces of foams.

Acknowledgments

The Research Council of Norway is acknowledged for the support to the PETROMAKS2 Project Durable Arctic Icephobic Materials (project no. 255507) and for the support to the Norwegian Micro- and Nano-Fabrication Facility, NorFab (project no. 245963).

References

1. Golovin, K.; Tuteja, A., A predictive framework for the design and fabrication of icephobic polymers. *Science Advances* **2017,** *3* (9), e1701617.

2. Zhuo, Y.; Hakonsen, V.; He, Z.; Xiao, S.; He, J.; Zhang, Z., Enhancing the mechanical durability of icephobic surfaces by introducing autonomous self-healing function. *ACS Applied Materials & Interfaces* **2018,** *10* (14), 11972-11978.

3. Golovin, K.; Dhyani, A.; Thouless, M. D.; Tuteja, A., Low–interfacial toughness materials for effective large-scale deicing. *Science* **2019,** *364* (6438), 371-375.

4. Gao, S.; Liu, B.; Peng, J.; Zhu, K.; Zhao, Y.; Li, X.; Yuan, X., Icephobic Durability of Branched PDMS Slippage Coatings Co-Cross-Linked by Functionalized POSS. *ACS Applied Materials & Interfaces* **2019,** *11* (4), 4654-4666.

5. Li, Q.; Guo, Z. G., Fundamentals of icing and common strategies for designing biomimetic anti-icing surfaces. *Journal of Materials Chemistry A* **2018,** *6* (28), 13549-13581.

6. Beemer, D. L.; Wang, W.; Kota, A. K., Durable gels with ultra-low adhesion to ice. *Journal of Materials Chemistry A* **2016,** *4* (47), 18253-18258.

7. Graeber, G.; Schutzius, T. M.; Eghlidi, H.; Poulikakos, D., Spontaneous self-dislodging of freezing water droplets and the role of wettability. *PNAS* **2017,** *114* (42), 11040-11045.

8. Guo, P.; Zheng, Y.; Wen, M.; Song, C.; Lin, Y.; Jiang, L., Icephobic/anti-icing properties of micro/nanostructured surfaces. *Advanced Materials* **2012,** *24* (19), 2642-2648.

9. Ramakrishna, D. M.; Viraraghavan, T., Environmental impact of chemical deicers - A review. *Water Air and Soil Pollution* **2005,** *166* (1-4), 49-63.

10. Wang, C.; Fuller, T.; Zhang, W.; Wynne, K. J., Thickness dependence of ice removal stress for a polydimethylsiloxane nanocomposite: Sylgard 184. *Langmuir* **2014,** *30* (43), 12819-12826.

11. Golovin, K.; Kobaku, S. P.; Lee, D. H.; DiLoreto, E. T.; Mabry, J. M.; Tuteja, A., Designing durable icephobic surfaces. *Science Advances* **2016,** *2* (3), e1501496.

12. He, Z.; Xiao, S.; Gao, H.; He, J.; Zhang, Z., Multiscale crack initiator promoted super-low ice adhesion surfaces. *Soft Matter* **2017,** *13* (37), 6562-6568.

13. Lv, J.; Song, Y.; Jiang, L.; Wang, J., Bio-inspired strategies for anti-icing. *ACS Nano* **2014,** *8* (4), 3152-3169.

14. He, Z.; Xie, W. J.; Liu, Z.; Liu, G.; Wang, Z.; Gao, Y. Q.; Wang, J., Tuning ice nucleation with counterions on polyelectrolyte brush surfaces. *Science Advances* **2016,** *2* (6), e1600345.

15. Zhu, K.; Li, X.; Su, J.; Li, H.; Zhao, Y.; Yuan, X., Improvement of anti-icing properties of low surface energy coatings by introducing phase-change microcapsules. *Polymer Engineering & Science* **2018,** *58* (6), 973-979.

16. Duan, C.; Zhu, Y.; Gu, W.; Li, M.; Zhao, D.; Zhao, Z.; Chen, Y.; Wang, Y., Atomic Coupling Growth of Graphene on Carbon Steel for Exceptional Anti-Icing Performance. *ACS Sustainable Chemistry & Engineering* **2018,** *6* (12), 17359-17367.

17. Zheng, S.; Bellido-Aguilar, D. A.; Wu, X.; Zhan, X.; Huang, Y.; Zeng, X.; Zhang, Q.; Chen, Z., Durable Waterborne Hydrophobic Bio-Epoxy Coating with Improved Anti-Icing and Self-Cleaning Performance. *ACS Sustainable Chemistry & Engineering* **2019,** *7* (1), 641-649.

18. Yamazaki, T.; Tenjimbayashi, M.; Manabe, K.; Moriya, T.; Nakamura, H.; Nakamura, T.; Matsubayashi, T.; Tsuge, Y.; Shiratori, S., Antifreeze Liquid-Infused Surface with High Transparency, Low Ice Adhesion Strength, and Antifrosting Properties Fabricated through a Spray Layer-by-Layer Method. *Industrial & Engineering Chemistry Research* **2019,** *58* (6), 2225-2234.

19. Chatterjee, R.; Beysens, D.; Anand, S., Delaying Ice and Frost Formation Using Phase-Switching Liquids. *Advanced Materials* **2019,** *31* (17), 1807812.

20. Yu, Y.; Jin, B.; Jamil, M. I.; Cheng, D.; Zhang, Q.; Zhan, X.; Chen, F., Highly Stable Amphiphilic Organogel with Exceptional Anti-icing Performance. *ACS Applied Materials & Interfaces* **2019,** *11* (13), 12838-12845.

21. Graeber, G.; Martin Kieliger, O. B.; Schutzius, T. M.; Poulikakos, D., 3D-Printed Surface Architecture Enhancing Superhydrophobicity and Viscous Droplet Repellency. *ACS Applied Materials & Interfaces* **2018,** *10* (49), 43275-43281.

22. Sandhu, A.; Walker, O. J.; Nistal, A.; Choy, K. L.; Clancy, A. J., Perfluoroalkane wax infused gels for effective, regenerating, anti-icing surfaces. *Chemical Communications* **2019,** *55* (22), 3215-3218.

23. Nosonovsky, M.; Hejazi, V., Why superhydrophobic surfaces are not always icephobic. *ACS Nano* **2012,** *6* (10), 8488-8491.

24. Varanasi, K. K.; Deng, T.; Smith, J. D.; Hsu, M.; Bhate, N., Frost formation and ice adhesion on superhydrophobic surfaces. *Applied Physics Letters* **2010,** *97* (23), 234102.

25. Karmouch, R.; Ross, G. G., Superhydrophobic wind turbine blade surfaces obtained by a simple deposition of silica nanoparticles embedded in epoxy. *Applied Surface Science* **2010,** *257* (3), 665-669.

26. Coady, M. J.; Wood, M.; Wallace, G. Q.; Nielsen, K. E.; Kietzig, A. M.; Lagugne-Labarthet, F.; Ragogna, P. J., Icephobic behavior of UV-Cured polymer networks incorporated into slippery lubricant-infused porous surfaces: improving SLIPS durability. *ACS Applied Materials & Interfaces* **2018,** *10* (3), 2890-2896.

27. Zheng, H. K.; Chang, S. N.; Zhao, Y. Y., Anti-Icing & Icephobic Mechanism and Applications of Superhydrophobic/Ultra Slippery Surface. *Progress in Chemistry* **2017,** *29* (1), 102-118.

28. Kim, P.; Wong, T. S.; Alvarenga, J.; Kreder, M. J.; Adorno-Martinez, W. E.; Aizenberg, J., Liquid-infused nanostructured surfaces with extreme anti-ice and anti-frost performance. *ACS Nano* **2012,** *6* (8), 6569-6577.

29. Liu, B.; Zhang, K. Q.; Tao, C.; Zhao, Y. H.; Li, X. H.; Zhu, K. Y.; Yuan, X. Y., Strategies for anti-icing: low surface energy or liquid-infused? *Rsc Advances* **2016,** *6* (74), 70251-70260.

30. Liu, M. M.; Hou, Y. Y.; Li, J.; Tie, L.; Guo, Z. G., Transparent slippery liquid-infused nanoparticulate coatings. *Chemical Engineering Journal* **2018,** *337*, 462-470.

31. Zhu, X.; Lu, J.; Li, X.; Wang, B.; Song, Y.; Miao, X.; Wang, Z.; Ren, G., Simple Way to a Slippery Lubricant Impregnated Coating with Ultrastability and Self-Replenishment Property. *Industrial & Engineering Chemistry Research* **2019,** *58* (19), 8148-8153.

32. Krongauz, V. V., Crosslink density dependence of polymer degradation kinetics: Photocrosslinked acrylates. *Thermochimica Acta* **2010,** *503*, 70-84.

33. Bartenev, G. M., Viscous flow and structure of linear polymers. *Journal of Polymer Science Part A-1: Polymer Chemistry* **1970,** *8* (12), 3417-3427.

34. He, Z.; Zhuo, Y.; He, J.; Zhang, Z., Design and preparation of sandwich-like polydimethylsiloxane (PDMS) sponges with super-low ice adhesion. *Soft Matter* **2018,** *14* (23), 4846-4851.

35. Wang, M.; Pan, N., Predictions of effective physical properties of complex multiphase materials. *Materials Science and Engineering: R: Reports* **2008,** *63* (1), 1-30.

36. Huang, C.; Bian, Z. G.; Fang, C. F.; Zhou, X. L.; Song, J. Z., Experimental and Theoretical Study on Mechanical Properties of Porous PDMS. *Journal of Applied Mechanics* **2018,** *85* (4), 041009.

37. Makkonen, L., Ice Adhesion - Theory, Measurements and Countermeasures. *Journal of Adhesion Science and Technology* **2012,** *26* (4-5), 413-445.

38. Lee, J. N.; Park, C.; Whitesides, G. M., Solvent compatibility of poly(dimethylsiloxane)-based microfluidic devices. *Analytical Chemistry* **2003,** *75* (23), 6544-6554.

39. Gao, X.; Diniz da Costa, J. C.; Bhatia, S. K., Understanding the diffusional tortuosity of porous materials: An effective medium theory perspective. *Chemical Engineering Science* **2014,** *110*, 55-71.

40. Zhu, D. Y.; Handschuh-Wang, S.; Zhou, X. C., Recent progress in fabrication and application of polydimethylsiloxane sponges. *Journal of Materials Chemistry A* **2017,** *5* (32), 16467-16497.

41. Andrews, E. H.; Majid, H. A.; Lockington, N. A., Adhesion of Ice to a Flexible Substrate. *Journal of Materials Science* **1984,** *19* (1), 73-81.

42. Bascom, W. D.; Cottington, R. L.; Jones, R. L.; Peyser, P., The fracture of epoxy- and elastomer-modified epoxy polymers in bulk and as adhesives. *Journal of Applied Polymer Science* **1975,** *19* (9), 2545-2562.

43. Kendall, K., The adhesion and surface energy of elastic solids. *Journal of Physics D: Applied Physics* **1971,** *4* (8), 1186-1195.

Table and Figures

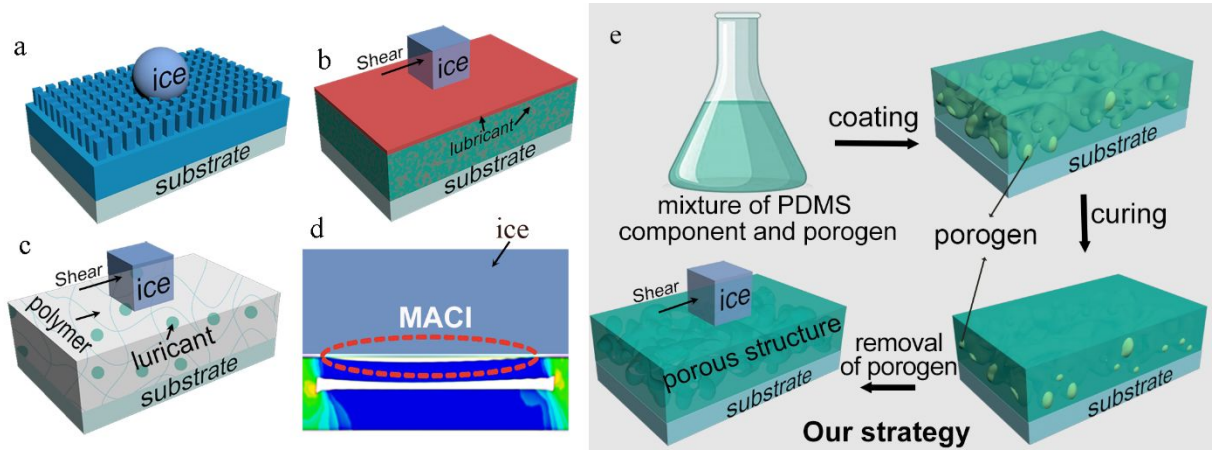

Figure 1 Schematic of reported icephobic surfaces by (a) superhydrophobic, (b) slippery, (c) interfacial slippage, (d) macroscale-initiator (MACI) mechanism,[15] (e) fabrication route of the present submicron porous elastomeric strategy for icephobicity.

Table 1 Parameters and properties of submicron porous foams prepared from varied weight ratio of porogen.

Samples	Porosity (%)	Pore size* (nm)	Unloading stiffness (N/m)	Reduced modulus (kPa)	Shear modulus (kPa)	τ_{ice} (kPa)
0%	0	-	171.1	3186	797	195.6 ± 26.0
10%	12.1 ± 4.5	489.6 ± 134.3	74.3	1383	370	124 ± 27.2
20%	18.8 ± 3.7	482.6 ± 144.5	66.0	1229	339	108 ± 19.1
30%	28.3 ± 1.9	483.9 ± 154.6	56.1	1045	299	72.8 ± 11.7
40%	42.1 ± 2.4	470.7 ± 134.6	52.7	981	292	40.7± 20.2
50%	48.4 ± 1.6	609.9 ± 96.6	48.5	903	272	-

*it represents the size distribution from the cross-sectional images of the foams.

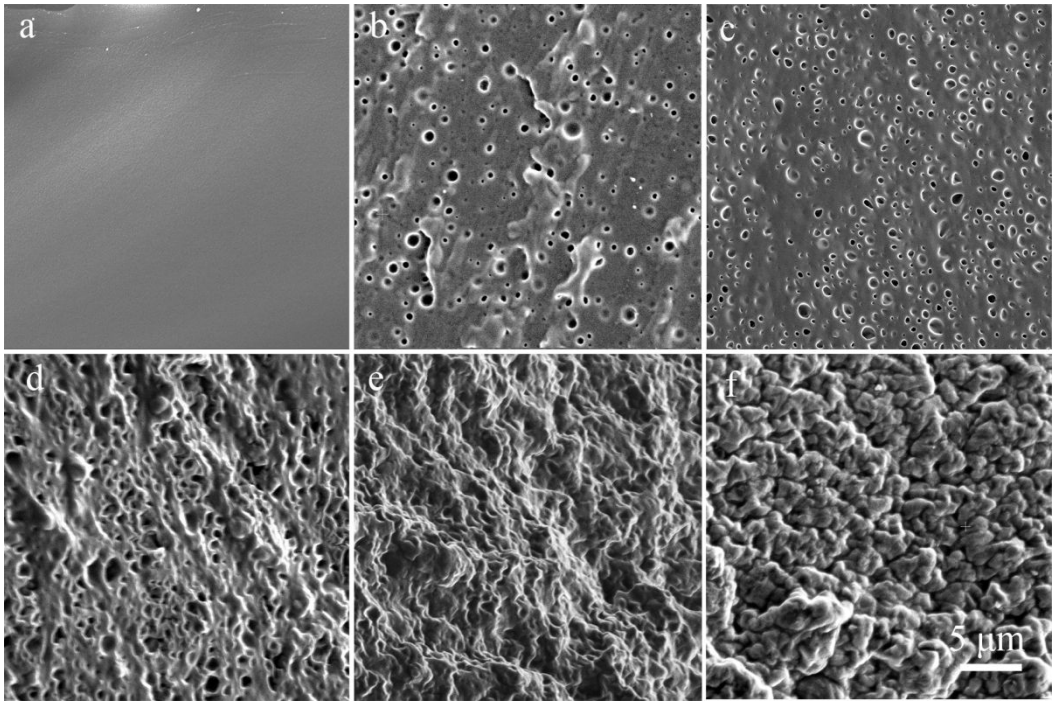

Figure 2 Cross-sectional SEM images of (a) pristine Sylgard 184, (b) 10%, (c) 20%, (d) 30%, (e) 40% and (f) 50% foams. With the increase of porogen, the porogen parts of the samples change from isolated to continuous structures.

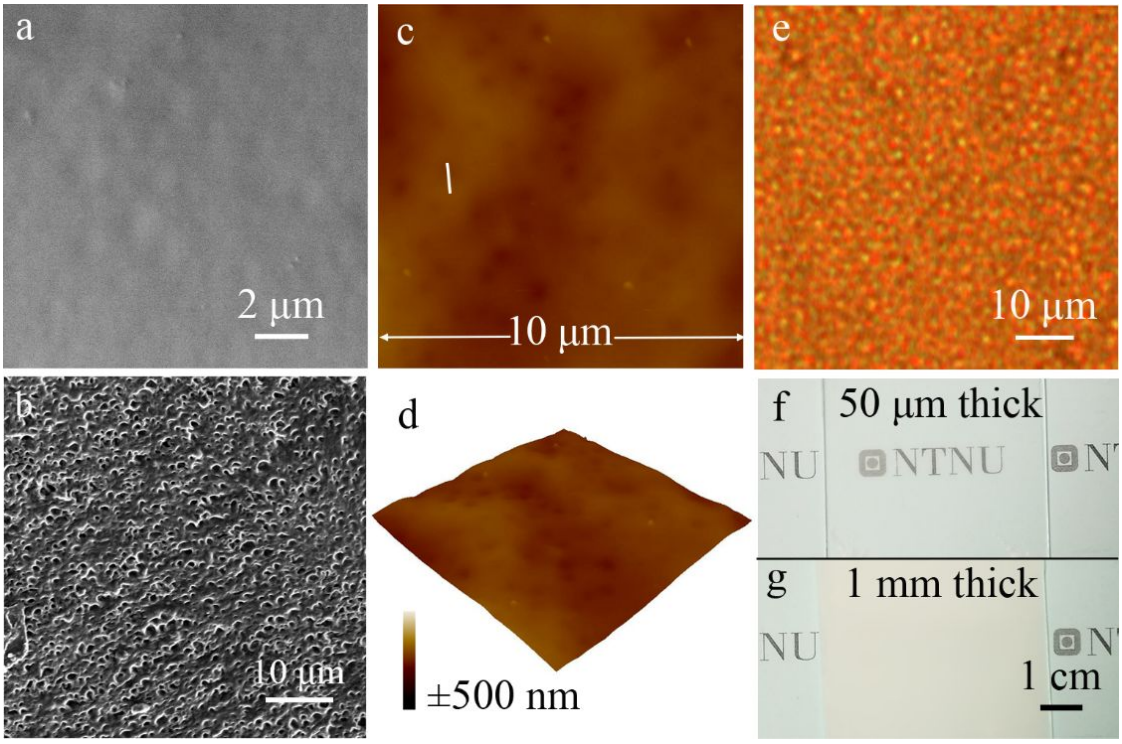

Figure 3 (a) Top-view and (b) cross-sectional SEM images of the 30% sample. (c) Two- and (d) three-dimensional AFM images of the 30% sample. (e-g) Optical microcopy images of the 30% sample.

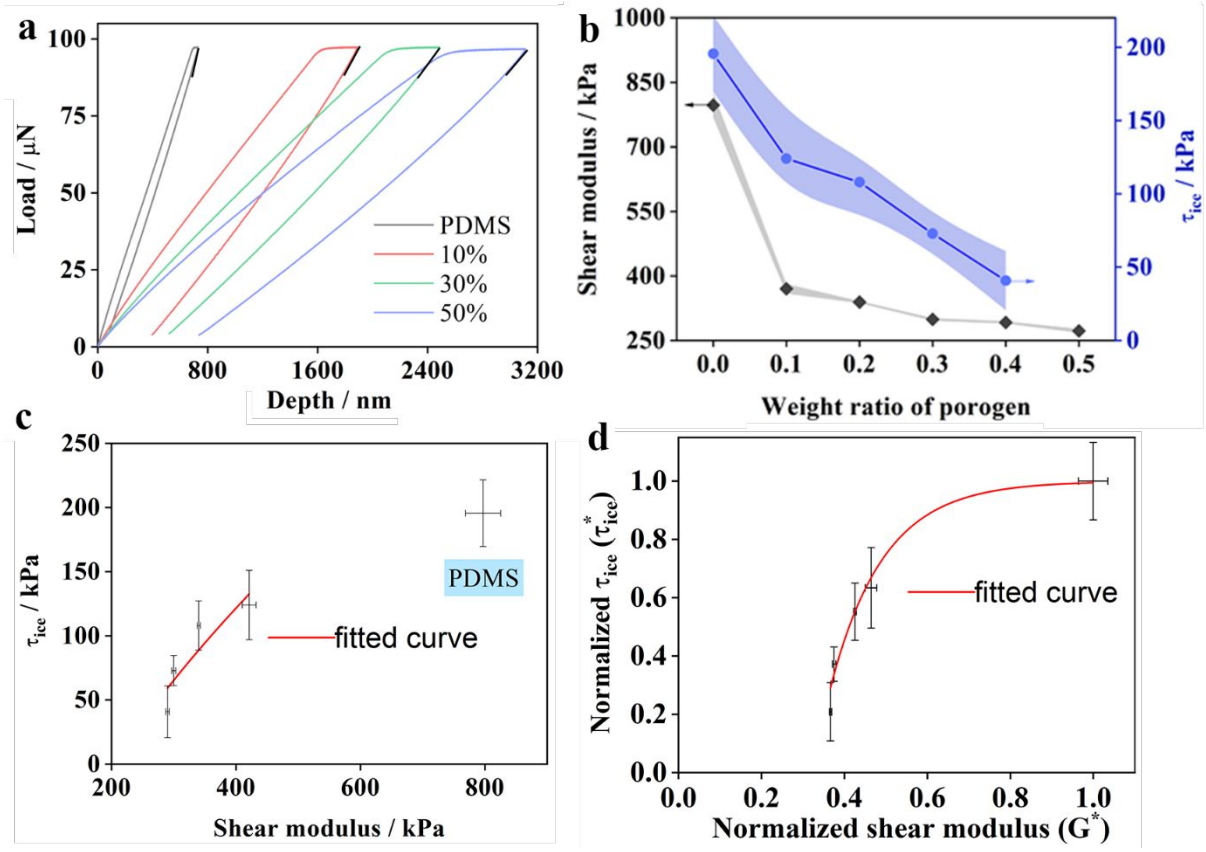

Figure 4 (a) Load-displacement curves, (b) relationship between apparent shear modulus/ice adhesion strength and weight ratio of porogen, (c) relationship between apparent shear modulus and ice adhesion strengths, and (d) relationship between normalized shear modulus and normalized ice adhesion strength for pristine Sylgard 184 and submicron porous coatings with thickness of *ca.* 50 μm. The percentage in Figure 4a represents the weight ratio of porogen used for preparing the foams. The black and blue regions in Figure 4b represent the error bars of the corresponding results.

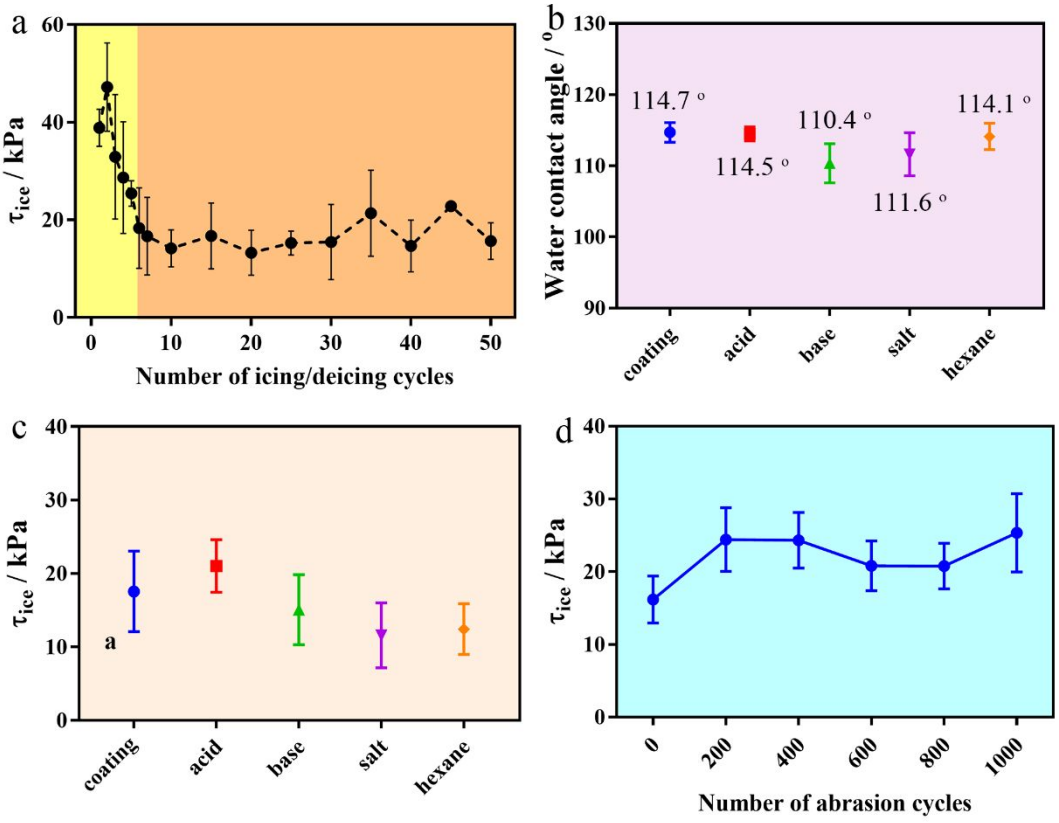

Figure 5 (a) Ice adhesion strengths of the submicron porous foam during the icing/deicing cycle tests. (b) Ice adhesion strengths and (c) water contact angles of the submicron foams before and after soaking by different liquid. (d) The ice adhesion strengths as a function of abrasion cycles.

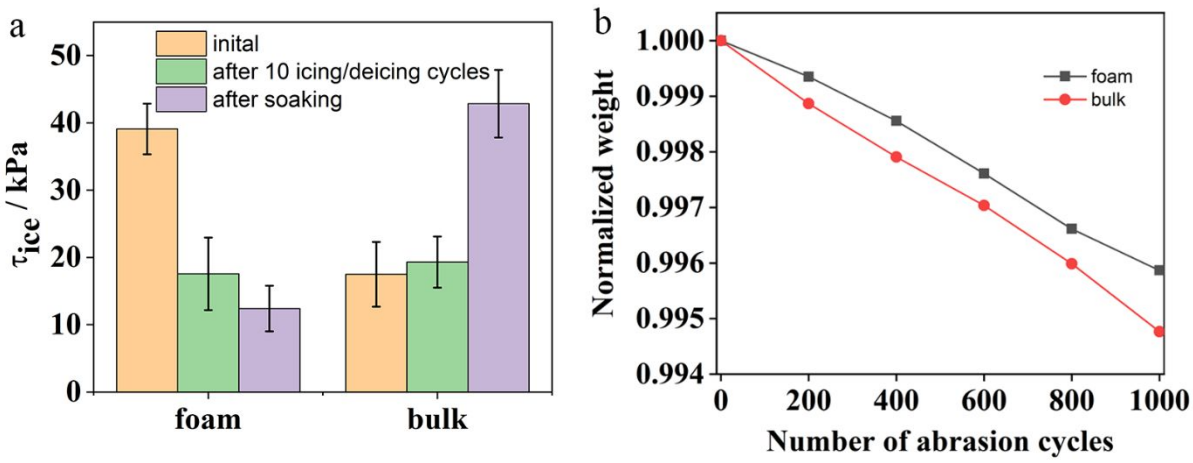

Figure 6 (a) Ice adhesion of foam and bulk PDMS before and after soaking in the organic solvent as well as after icing/deicing cycles. (b) Normalized weight loss of foam and bulk PDMS as a function of number of abrasion cycles.

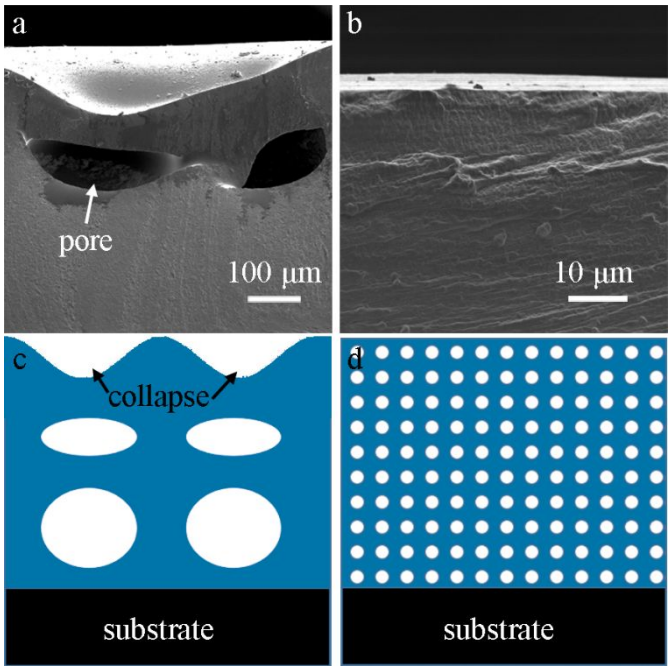

Figure 7 Cross-sectional SEM images and corresponding schematic of deformation performance for foams with sub-millimetric (a,c) and submicron porous structures (b,d).